High Frequency Torque Ripple Mitigation and Available Torque Limit Extension in Signal-Injection Sensorless Control Method

Abstract— This paper proposes a sensorless control method for interior permanent magnet synchronous motor (IPMSM) with minimized high frequency (HF) torque ripple in the entire torque region. Accordingly, HF voltage is injected into the specific axis to mitigate HF torque ripple. The current observation angle and compensation component are exploited to enhance the stability of the signal injection sensorless algorithm at a high torque region. The estimated rotor position tracks the rotor position under the high torque region, and the HF torque ripple is mitigated with the proposed method. Simulations and experiments verified the superiority of the proposed method.

I. INTRODUCTION

For the vector control of the interior permanent magnet synchronous motor (IPMSM), the rotor position should be measured precisely with the position sensor. However, the use of sensors makes the volume of the drive system bulky, increasing the total cost and complexity of the system. Therefore, research regarding the sensorless control of the motor has been conducted [1]-[5]. Among them, for the case of high frequency (HF) signal injection sensorless control (SISC), HF torque ripple is induced in response to the injected HF voltage. This HF torque ripple causes the actual acoustic noise making the users uncomfortable. In order to minimize HF torque ripple, recent research has been implemented to design a new injection voltage signal [2]-[3]. However, the convergence characteristics of the methods can deteriorate in the high torque region because the nonlinearity caused by magnetic saturation of the motor core and spatial harmonic is not considered [4].

This paper proposes a new method to enhance the stability of the SISC method in the entire torque region. The HF voltage equation of IPMSM is modeled considering the nonlinear relationship between the magnetic flux linkage and the stator current. The method to obtain HF voltage injection angle that mitigates HF torque ripple is introduced. Based on this analysis, a current signal processing method to extend the available torque region is proposed. Experiments and simulations verify the proposed method.

II. HIGH FREQUENCY TORQUE RIPPLE MITIGATION

A. High Frequency Component Model

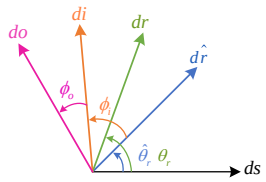

Fig. 1. Definition of reference frames and angles.

Fig. 1 shows the reference frames and angles discussed in this paper. *dr*-axis is aligned along the flux linkage of the permanent magnet in the IPMSM, and *qr*-axis is electrically 90º ahead of *dr*-axis. θ_r and $\hat{\theta}_r$ represent the actual rotor position and the estimated rotor position, respectively. ϕ_i and ϕ_o are the voltage injection angle and the current observation angle, which are used for defining ancillary reference frames. *di* and *do* axes represent *d*-axis of ancillary injection reference frame (AIRF) and ancillary observation reference frame (AORF), respectively.

In the conventional method, HF voltage signal is injected into $d\hat{r}$ axis, and $q\hat{r}$ axis HF current signal is processed to derive the position-tracking observer's input [5]. However, to minimize HF torque ripple, a proper AIRF is selected. The injected HF voltage can be expressed as follows:

$$\mathbf{v}_{\mathbf{dqsh}}^{\mathbf{i}\,*}[n] = \begin{bmatrix} V_h \\ 0 \end{bmatrix} \cdot clk[n]\,. \tag{1}$$

In (1), $\mathbf{v}$ denotes voltage vector and its superscript '*i*', subscript '*s*', and '*h*' refer to AIRF, stator component, and HF component, respectively. V_h is an amplitude of HF injection voltage and $clk[n]$ is a signal that pulsates with +1 and -1 at each sampling interval, T_s. The superscript '*' refers to the reference. The torque of IPMSM is modeled by $T_e(i_{ds}^r, i_{qs}^r)$. *i* denotes current and superscript '*r*' stands for rotor reference frame (RRF). The instantaneous torque of IPMSM is also affected by rotor position; however, it can be expressed with a function of stator current if the effect of spatial harmonic is ignored.

The HF voltage equation can be derived with the small-signal approximation at the specific current operating point as follows:

$$\mathbf{v}_{\mathbf{dqsh}}^{\mathbf{r}} = \begin{bmatrix} v_{dsh}^r \\ v_{qsh}^r \end{bmatrix} = \begin{bmatrix} L_{dh} & L_{dqh} \\ L_{qdh} & L_{qh} \end{bmatrix} \frac{d}{dt} \begin{bmatrix} i_{dsh}^r \\ i_{qsh}^r \end{bmatrix}. \quad (2)$$

In (2), L_{dh} and L_{qh} stand for HF inductances of d and q axis, which are $\partial\lambda_{ds}^r / \partial i_{ds}^r$ and $\partial\lambda_{qs}^r / \partial i_{qs}^r$, respectively. L_{dqh} and L_{qdh} stand for mutual HF inductances, which are $\partial\lambda_{ds}^r / \partial i_{qs}^r$ and $\partial\lambda_{qs}^r / \partial i_{ds}^r$. λ stands for magnetic flux. The nonlinearity of HF inductance according to magnetic flux saturation is considered in this paper. The voltage drop due to the stator resistance can be ignored, and the time derivative of flux linkage is dominant over the other components. Assuming the actual angle is well estimated ($\tilde{\theta}_r = \theta_r - \hat{\theta}_r \approx 0$), HF current variation according to HF voltage injected into AIRF is as follows:

$$\Delta\hat{\mathbf{i}}_{\mathbf{dqsh}}^{\hat{\mathbf{r}}}[n] \approx \Delta\mathbf{i}_{\mathbf{dqsh}}^{\mathbf{r}}[n] = \begin{bmatrix} \Delta i_{dsh}^r[n] \\ \Delta i_{qsh}^r[n] \end{bmatrix} = \begin{bmatrix} I_\Sigma \cos\phi_i + I_\Delta \cos(2\phi_\Delta + \phi_i) \\ I_\Sigma \sin\phi_i - I_\Delta \sin(2\phi_\Delta + \phi_i) \end{bmatrix} \cdot clk[n]. \quad (3)$$

The superscript '$\hat{r}$' means ERRF. In (3), $I_\Sigma = \frac{V_h T_s \Sigma L_h}{L_{dh}L_{qh} - L_{dqh}^2}$, $I_\Delta = \frac{V_h T_s \sqrt{L_{dqh}^2 + \Delta L_h^2}}{L_{dh}L_{qh} - L_{dqh}^2}$, $\phi_\Delta = \frac{1}{2}\text{atan2}(L_{dqh}, -\Delta L_h)$, $\Sigma L_h \triangleq \frac{L_{dh} + L_{qh}}{2}$, and $\Delta L_h \triangleq \frac{L_{dh} - L_{qh}}{2}$. $\Delta\mathbf{i}_{\mathbf{dqsh}}^{\mathbf{r}}[n]$ and an absolute value of HF torque ripple ($\Delta T_e[n] = |T_e[n] - T_e[n-1]|$) depends on ϕ_i.

B. HF torque ripple mitigation

Table I. ΔT_e at 0 pu, 1pu, and 2 pu torque according to ϕ_i = 0°, 10°, and 20°.

T_e^* \ ϕ_i	0°	10°	20°
0 pu	0.00461	0.05455	0.09999
1 pu	0.02966	0.05245	0.12452
2 pu	0.6511	0.0458	0.13709

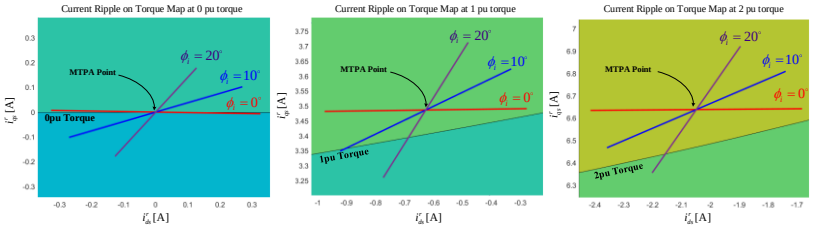

(a) (b) (c)

Fig. 2. HF current trajectories on the torque map at (a) 0 pu, (b) 1 pu, and (c) 2 pu torque.

Fig. 2 shows the torque map with the trajectory of the HF current variation at 0 pu, 1 pu, and 2 pu torque. Table I represents ΔT_e according to ϕ_i at each torque reference. In this case, the injected voltage and frequency are set to V_h =40 V, f_h =5 kHz, respectively. Averaged torque data is employed in Fig. 2. As shown in Fig. 2 and Table I, the trajectory of the instantaneous current varies according to ϕ_i at steady-state. Accordingly, the responding HF torque ripple is changed by ϕ_i. The relationship between HF torque ripple and HF current variation can be assumed as linear and represented as follows:

$$T_e(i_{ds}^r, i_{qs}^r) = \nabla T_e(i_{dsf}^r, i_{qsf}^r) \cdot \begin{bmatrix} i_{ds}^r - i_{dsf}^r \\ i_{qs}^r - i_{qsf}^r \end{bmatrix} + T_e(i_{dsf}^r, i_{qsf}^r). \quad (4)$$

The subscript 'f' refers to the fundamental component. The HF torque ripple can be minimized to 0 only when $\nabla T_e(i_{dsf}^r, i_{qsf}^r)$ and $\Delta\mathbf{i}_{\mathbf{dqsh}}^{\mathbf{r}}[n]$ are perpendicular at $\phi_i = \text{atan}\left(\frac{I_\Sigma + I_\Delta \cos 2\phi_\Delta - mI_\Delta \sin 2\phi_\Delta}{I_\Delta \sin 2\phi_\Delta - mI_\Sigma + mI_\Delta \cos 2\phi_\Delta}\right)$, where $m = \frac{\partial T_e / \partial i_{qs}^r}{\partial T_e / \partial i_{ds}^r}$ at $i_{ds}^r = i_{dsf}^r$ and $i_{qs}^r = i_{qsf}^r$.

III. AVAILABLE TORQUE LIMIT EXTENSION

Fig. 3 shows the block diagram of the proposed SISC algorithm. The superscript 's' refers to stationary reference frame. In [3]-[4], to minimize HF torque ripple, the difference of q-axis current in AIRF is used to estimate the position error. However, this paper proposes a signal processing method where the q-axis current component of AORF is exploited for signal processing.

The HF current component in AORF is expressed as follows:

$$\Delta \mathbf{i}^{o}_{dqsh}[n] = \mathbf{R}(-\phi_o)\Delta \mathbf{i}^{i}_{dqsh}[n] = \begin{bmatrix} I_\Sigma \cos\phi_o + I_\Delta \cos(2\tilde{\theta}_r - 2\phi_\Delta - 2\phi_i - \phi_o) \\ -I_\Sigma \sin\phi_o + I_\Delta \sin(2\tilde{\theta}_r - 2\phi_\Delta - 2\phi_i - \phi_o) \end{bmatrix} \cdot clk[n]. \quad (5)$$

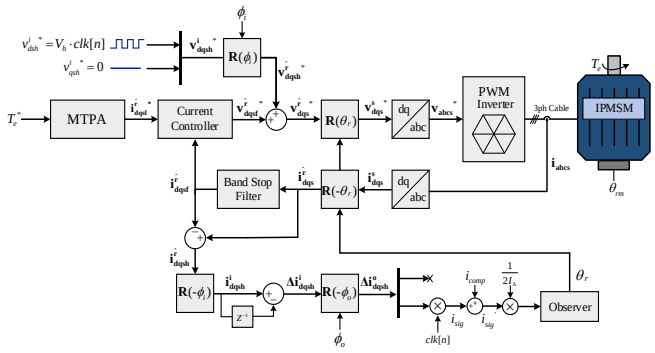

Fig. 3. Block diagram of proposed SISC algorithm.

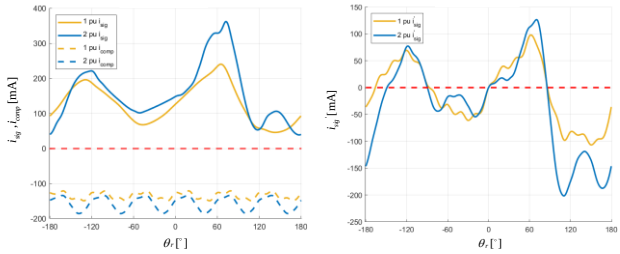

(a) (b)

Fig. 4. (a) i_{sig} and i_{comp} curves at $\theta_r = 50°$ and (b) i_{sig}' curves at $\theta_r = 50°$ with convergence point manipulation.

To extract the input of the position tracking observer, estimated position error ($\tilde{\theta}_{r,est}$), i_{sig} can be set as $i_{sig} = \Delta i^{o}_{qsh}[n] \cdot clk[n]$ and expressed as

$$i_{sig} = -I_\Sigma \sin\phi_o + I_\Delta \sin(2\tilde{\theta}_r - 2\phi_\Delta - 2\phi_i - \phi_o). \quad (6)$$

Due to the negative feedback of the observer, the convergence point of $\tilde{\theta}_r$ is determined with the zero up-crossing point where $i_{sig} = 0$ with $\partial i_{sig} / \partial \tilde{\theta}_r > 0$. However, if the i_{sig} in (6) is employed, the convergence point can be far from the desired convergence point where $\tilde{\theta}_r = 0$. Therefore, to manipulate the convergence point into the desired convergence point, the following equations are exploited:

$$i_{comp} = -i_{sig}(\tilde{\theta}_r = 0, \theta_r = \hat{\theta}_r) \quad (7)$$

$$\text{and } i_{sig}' = i_{sig} + i_{comp}. \quad (8)$$

In the proposed method, i_{sig}' is used as an input of the observer instead of i_{sig}. Assumed that the inductances are constant regardless of the rotor position and the current operating point, the following equation is derived:

$$i_{sig}' = I_\Delta \sin\left(2\tilde{\theta}_r - 2\phi_\Delta - 2\phi_i - \phi_o\right) + I_\Delta \sin\left(2\phi_\Delta + 2\phi_i + \phi_o\right). \quad (9)$$

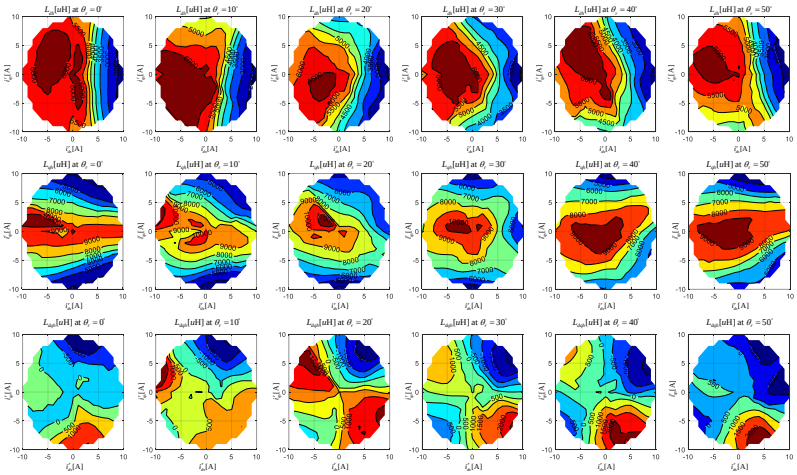

Fig. 5. Contour maps of L_{dh}, L_{qh}, and L_{dqh} extracted with experiment according to i^r_{ds}, i^r_{qs}, and θ_r.

If the observation angle is set with $\phi_o = -2\phi_\Delta - 2\phi_i$, i_{sig}' can be approximated to $I_\Delta \sin(2\tilde{\theta}_r)$. Under this condition, the convergence point of i_{sig}' is set to the desired convergence point. However, the nonlinearity between flux linkage and stator current should be dealt with in the high torque region. For this, an index is defined as follows:

$$\theta_{Conv} \triangleq \min(|\tilde{\theta}_r|) \quad \text{s.t.} \quad i_{sig}' = 0 \text{ except } \tilde{\theta}_r = 0 \text{ for } 0 \le \theta_r < 60° \quad (10)$$

Physically, if $\tilde{\theta}_r$ exists from $-\theta_{Conv}$ to θ_{Conv}, $\tilde{\theta}_r$ moves towards 0°. Therefore, the stability of convergence can be enhanced by larger θ_{Conv}. The convergence characteristic can be highly improved by setting θ_{Conv} to the maximum value of 90° when $i_{sig}' = I_\Delta \sin(2\tilde{\theta}_r)$. Fig. 4 depicts i_{sig}, i_{comp}, and i_{sig}' according to $\tilde{\theta}_r$ at $\theta_r = 50°$ when the torque is set with 1 pu and 2 pu. As shown in Fig. 4(a), i_{sig} has no zero-up crossing points at both 1 pu and 2 pu torque. Therefore, $\tilde{\theta}_r$ does not converge if i_{sig} itself is processed for $\tilde{\theta}_{r,est}$. However, $\tilde{\theta}_r$ converges to 0° and θ_{Conv} is extended close

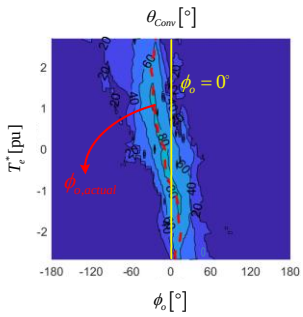

Fig. 6. θ_{Conv} contour map according to T_e^* and ϕ_o.

to 90º if i_{sig}' is employed for constructing the observer input as shown in Fig. 4(b). However, ϕ_o should be obtained considering saturation and spatial harmonics. As shown in Fig. 5, HF inductances have different values for each stator current and the rotor position because of the magnetic saturation of the core and spatial harmonic components. For all T_e^*, θ_{Conv} is calculated according to ϕ_o. ϕ_o which maximizes θ_{Conv} is chosen for the proposed method. This process in this paper was conducted with MATLAB simulation.

Fig. 6 shows a contour map of θ_{Conv} according to T_e^* and ϕ_o. ϕ_o which maximizes θ_{Conv} at each T_e^* is represented with the red line. The yellow line depicts the line where $\phi_o = 0$. It is expected that the convergence characteristic of $\tilde{\theta}_r$ over 1 pu region will be degraded if ϕ_o is set to 0º because of the low θ_{Conv}. Fig. 7 shows contour maps of i_{sig} and i_{sig}' with 3 methods: method A [5], method B [3], and the proposed method. Method B corresponds to the yellow line in Fig. 6. Red lines in contour maps are composed of the points where i_{sig} or i_{sig}' is 0. The convergence points in Fig. 7(a) are not placed at $\tilde{\theta}_r = 0$, but those in Fig. 7(b) are. However, Fig. 7(b) shows that the convergence characteristic becomes highly undermined in the high torque region of 1.3 pu or more due to low θ_{Conv}. In Fig. 7(c), the convergence characteristic is enhanced in the proposed method since θ_{Conv} is larger than 80º at the entire torque region. Therefore, the available torque region is extended with the proposed method.

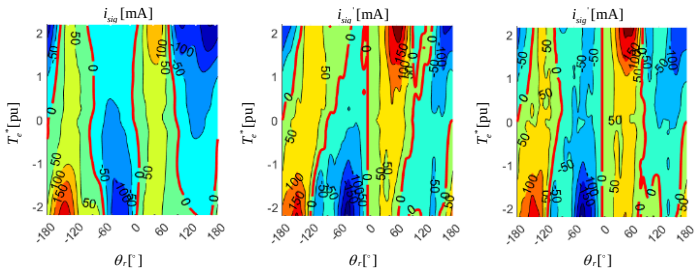

Fig. 7. i_{sig} and i_{sig}' contour maps (a) with method A [5], (b) with method B [3], and (c) with the proposed method at $\theta_r = 40°$.

IV. Conclusion

This paper analyzes HF torque ripple and convergence characteristics of IPMSM SISC. The analytic solution of injection angle that mitigates HF torque ripple is proposed. Compensation current is employed to manipulate the convergence point to improve position-tracking performance. Moreover, the observation angle is used to extend the available torque limit. This observation angle is numerically obtained by considering the nonlinear relationship between flux linkage and stator current. With the proposed method, the observer can precisely track the actual position for the entire torque region with minimized HF torque ripple. **The experimental results will be accompanied by the full paper.**

References

[1]G. Xie, K. Lu, S. K. Dwivedi, J. R. Rosholm and F. Blaabjerg, "Minimum-Voltage Vector Injection Method for Sensorless Control of PMSM for Low-Speed Operations," *IEEE Trans. Power Electron.*, vol. 31, no. 2, pp. 1785-1794, Feb. 2016.

[2]C. Li, G. Wang, G. Zhang and D. Xu, "HF Torque Ripple Suppression for HF Signal Injection Based Sensorless Control of SynRMs," 2019 IEEE Applied Power Electronics Conference and Exposition (APEC), 2019, pp. 2544-2548.

[3]Z. Lin, X. Li, Z. Wang, T. Shi and C. Xia, "Minimization of Additional HF Torque Ripple for Square-Wave Voltage Injection IPMSM Sensorless Drives," *IEEE Trans. Power Electron.*, vol. 35, no. 12, pp. 13345-13355, Dec. 2020.

[4]Y. -C. Kwon, J. Lee and S. -K. Sul, "Extending Operational Limit of IPMSM in Signal-Injection Sensorless Control by Manipulation of Convergence Point," *IEEE Trans. Ind.*, vol. 55, no. 2, pp. 1574-1586, Mar.-Apr. 2019.

[5]Y. -D. Yoon, S. -K. Sul, S. Morimoto and K. Ide, "High-Bandwidth Sensorless Algorithm for AC Machines Based on Square-Wave-Type Voltage Injection," *IEEE Trans. Ind.*, vol. 47, no. 3, pp. 1361-1370, May-June 2011.